# Influence of Plastic Deformation on Bimaterial Fault Rupture Directivity

Nora DeDontney[1], Elizabeth L. Templeton-Barrett[2], James R. Rice[1,3], Renata Dmowska[3]

**Abstract.** Material juxtapositions across mature faults are a common occurrence. Previous work has found that this elastic mismatch results in a rupture that will preferentially propagate in the direction of slip displacement on the more compliant side of the fault, with more off-fault damage in the stiffer material. This result has implications for inferring preferred rupture directions based on observations of damage zone asymmetry. We perform a complete numerical investigation of the role of the stress state on the distribution of plastic deformation and the direction of preferred rupture propagation. We show that there are important factors, in addition to the elastic mismatch, which control the preferred direction of propagation as well as the side of the fault in which damage predominately accumulates. The orientation of the most compressive principal stress is the controlling factor in determining the location of plastic deformation. For different orientations, plastic deformation can accumulate in either the stiffer or the more compliant material. For high angles of most compressive stress, the aforementioned preferred rupture direction prediction holds true. However, the off-fault plastic response can reverse that direction for low angles of most compressive stress so that rupture will preferentially propagate in the direction of slip displacement in the stiffer material.

## 1. Introduction

Previous work has found that an elastic mismatch across a fault can result in a rupture that preferentially propagates in the direction of slip displacement on the more compliant side of the fault [*Andrews and Ben-Zion*, 1997; *Ben-Zion and Andrews*, 1998; *Ben-Zion*, 2001]. *Andrews and Ben-Zion* [1997] and *Ben-Zion and Andrews* [1998] confirmed the existence of wrinkle-like slip pulses, postulated by *Weertman* [1980], that propagate unilaterally in the direction of slip in the more compliant medium, for a constant friction coefficient, due to a dynamic reduction of normal stress. More complete analyses [*Cochard and Rice*, 2000; *Adams*, 2001] based on *Adams* [1995], provided simple slip-pulse solutions propagating at the generalized Rayleigh wave speed for the bimaterial pair. *Cochard and Rice* [2000], based on *Ranjith and Rice* [2001], showed, for the case of constant friction coefficient and under special starting conditions, that a slip pulse solution was also possible propagating in the opposite direction, at a speed close to the dilatational wave speed of the more compliant material.

Alternatively, *Harris and Day* [1997] performed numerical simulations for bimaterial fault models with slip weakening of the friction coefficient. They observed bilateral ruptures, but noted asymmetries in the slip and rupture velocities in the two directions. *Harris and Day* [1997] also observed occasional transitions to supershear rupture in a direction opposite to that of slip displacement in the more compliant material. Those numerical observations are in agreement with the experimental work of *Xia et al.* [2005], who investigated the directionality of rupture on a bimaterial interface in the laboratory and found that for the conditions examined, rupture was always bilateral. *Xia et al.* [2005] observed that rupture was modestly faster in the Weertman "preferred" direction, so long as both fronts moved at sub-shear speeds, but in samples with increased shear prestress, rupture ultimately transitioned to a considerably faster, supershear rupture in the direction opposite to that "preferred" direction.

*Harris and Day* [2005] conducted 3-dimensional (3D) numerical investigations and examined small (M4-M6) earthquakes in Parkfield, California, where there is a material contrast across the San Andreas fault. *Harris and Day* [2005] found that rupture propagated in both directions in both the numerical models and the actual events. However, *Ben-Zion* [2006a] notes that these small events may be influenced by the local San Andreas fault structure, rather than the properties of the crustal blocks, and more observational constraints are needed. Additionally, *Harris and Day* [1997], *Harris and Day* [2005] and *Andrews and Harris* [2005] found, using 2-dimensional (2D) and 3D numerical models, that rupture is bilateral and that features like the wrinkle-like slip pulse are seen only near the rupture front. In contrast, *Ben-Zion* [2006b] conclude that there is a broad parameter range in which the wrinkle-like slip pulse is relevant. Additionally, *Dalguer and Day* [2009] show that variations in the depth and initial stress state of large aspect ratio faults can result in either unilateral or bilateral rupture propagation in an elastic medium, so additional 3D effects can alter these results.

We confirm here that the level of shear prestress, relative to peak strength, is an important factor in determining how the rupture propagates in a slip-weakening model; higher prestress allows a transition to supershear rupture in a direction opposite to what is normally called the "preferred" direction (and seems to be the direction with propagation near the generalized Rayleigh speed) at lower shear prestress.

[1]Department of Earth and Planetary Sciences, Harvard University, Cambridge, MA, 02138, USA.

[2]School of Engineering and Applied Sciences, Harvard University, now at ExxonMobil Upstream Research Company, Houston, TX, 77098, USA.

[3]School of Engineering and Applied Sciences, Harvard University, Cambridge, MA, 02138, USA.

1

In addition to the rupture directionality, we must also consider the generation of plastic deformation off of the fault. The asymmetry of damage accumulation due to the dynamic propagation of rupture through an elastic-plastic material has been widely modeled under a variety of conditions. There are two theories to explain what determines which side of the fault undergoes greater plastic deformation. Studies by *Poliakov et al.* [2002] and *Templeton and Rice* [2008], on homogeneous materials, suggest that the angle between the most compressive principal stress and the fault, $\Psi$, is the controlling factor and determines whether deformation accumulates in the compressive or extensional side of the fault. *Viesca et al.* [2008] extended this to examine the role of pore fluids and observed that an undrained, saturated material exhibits a wider or narrower zone of deformation, depending on $\Psi$. In contrast, studies by *Ben-Zion and Shi* [2005] examined the dynamic rupture propagation and resulting plastic deformation in the bulk and found that rupture only propagated in the direction of slip in the more compliant material when a bimaterial interface was considered. *Ben-Zion and Shi* [2005] also found that damage accumulated only in the stiffer medium with a faster seismic velocity. Their study was conducted, however, for only a single prestress orientation with maximum compression at $45°$ to the fault (plausible for the major California strike-slip faults studied).

*Dor et al.* [2006] applied the *Ben-Zion and Shi* [2005] concepts to the San Andreas, San Jacinto, and Punchbowl faults of southern California. They noted a large asymmetry in the observed damage pattern around these faults, with more damage located on the northeast side of the faults where higher wave speed materials (and thus stiffer material if density varies only modestly) were found. Applying the study of *Ben-Zion and Shi* [2005], they concluded that there was a preferred rupture propagation direction towards the northwest, along the faults studied.

While this conclusion seems valid for values of $\Psi$ close to $45°$, the work of *Templeton and Rice* [2006, 2008] suggests that the same conclusion might not be reached for some other ranges of prestress orientations. *Templeton and Rice* [2006, 2008] show that for high and low prestress angles, plastic deformation occurs on different sides of the fault and *Templeton and Rice* [2006] also examine the extent of plastic deformation when there is a material contrast across the fault. *Duan* [2008] show that for a high prestress angle, the accumulation of plastic deformation is asymmetric about the fault in the presence of a material contrast. Hence, a more complete study of the role of $\Psi$ in determining the distribution of off-fault deformation, for the case of a bimaterial interface, seems in order. The following discussion presents a detailed computational investigation into how stress orientation and magnitude control the preferred rupture propagation direction and location of plastic deformation in the bimaterial problem.

## 2. Model Setup

Analyses of right-lateral dynamic shear rupture in elastic and elastic-plastic media were conducted using the finite element code ABAQUS/Explicit. The fault is embedded in 2D plane strain finite elements and absorbing boundary conditions surround the entire model. The mesh utilizes larger elements far from the fault (figure 1), where no plastic deformation is expected, allowing for faster computation times, but the region shown in all figures is of the finest resolution.

A material contrast is prescribed across the fault, with a more compliant material, material 1, above the fault, and a stiffer material, material 2, below the fault (see table 1 for values). We use a wave speed contrast of 1.25, which is high when compared to the observation of 1.09 for the San Andreas fault [*Fuis et al.*, 2003], but not for other tectonic regimes with a material mismatch, such as a subduction zone [*Takahashi et al.*, 2002].

We neglect the effects of pore fluids here; if fluid-saturated, we may consider the initial stress state to be an effective stress state and neglect changes in pore pressure along the fault during dynamic rupture. An alternative simple interpretation of our results, based on *Viesca et al.* [2008], is that we assume an undrained elastic-plastic response on the seismic time scale, in which case simple formulae exist for transforming the elastic-plastic parameters used here between undrained and drained response as given by *Viesca et al.* [2008].

The model is initially loaded with a uniform stress state that is characterized by an orientation of the most compressive principal stress with the fault, $\Psi$, and an $S$ ratio, which characterizes how close the initial shear stress on the fault, $\tau^0$, is to failure. The $S$ ratio is defined by $S = (\tau^p - \tau^0)/(\tau^0 - \tau^r)$ [*Andrews*, 1976; *Das and Aki*, 1977], where $\tau^p$ and $\tau^r$ are the peak and residual strengths of the fault respectively. The peak and residual strengths are the product of the fault normal compressive stress and the static and dynamic coefficients of friction, respectively. In evaluating $S$, the normal stress is based on the initially uniform compressive normal stress (that stress is altered during dynamic rupture). A lower $S$ ratio indicates that the fault is closer to failure ($S = 0$ is at failure), and a higher $S$ ratio indicates that fault is further from failure.

We look at a range in values for $\Psi$ and $S$ with $\Psi = 15°$, $25°$, $35°$, $45°$ and $S = 0.8$, 1.4 and 2.0. Combinations of these result in the twelve stress states that are considered here. We do not show results for larger angles of $\Psi$ here, as we have found that $\Psi = 35°$ and $\Psi = 45°$ are representative of larger values for $\Psi$, and includes the $45°$ examined by *Ben-Zion and Shi* [2005].

### 2.1. Fault Frictional Behavior

We implement a slip-weakening formulation [*Ida*, 1972; *Palmer and Rice*, 1973], as described fully in *Templeton and Rice* [2008], in which the coefficient of friction, $f$, decays linearly from a peak static value, $f_s$, to a residual dynamic value, $f_d$, over a characteristic amount of slip, $D_c$.

A length scale that arises is the slip-weakening zone size, $R$, which, in the case of homogeneous media, depends on the rupture velocity, $V_r$, and decreases to zero at $V_r \to C_R$, where $C_R$ is the Rayleigh wave speed. At low rupture speeds and large $S$, $R \approx R_0$, and for rupture between identical materials, $R_0$ can be related to $D_c$ by [*Palmer and Rice*, 1973]

$$R_0 = \frac{9\pi}{32(1-\nu)} \frac{GD_c}{(f_s - f_d)\sigma_n} \qquad (1)$$

where $G$ is the shear modulus, $\nu$ is Poisson's ratio, and $\sigma_n$ is the fault normal stress ($\sigma_n$, positive in compression, is defined by $\sigma_n = -n_i\sigma_{ij}n_j$ for surface normal **n**). The theory is under development for the bimaterial case [*Hirano, S.* (2011), *personal communication*], so we use (1) to determine the ratio, $D_c/R_0$, implemented in the model, using the elastic material parameters of material 1. *Rice et al.* [2005] estimated that a representative value for $R_0$ is 20-40 m for the mid-seismogenic zone of crustal continental earthquakes. A resolution of 40 elements in $R_0$ is used in the vicinity of the faults to ensure that the slip-weakening process is well resolved. The characteristics of the rupture propagation are not significantly different for higher ($\Delta x = R_0/60$) or lower ($\Delta x = R_0/20$) resolutions, so we are adequately resolving the rupture process.

We implement a numerical regularization scheme because the bimaterial sliding problem is ill-posed. Sliding is unstable at constant friction values and as the wavelength of a perturbation decreases towards zero, the growth rate diverges

[e.g., *Renardy*, 1992; *Adams*, 1995; *Simones and Martins*, 1998]. We use the form

$$\frac{d\tau}{dt} = -\frac{1}{t^*}[\tau - f\sigma_{\mathbf{n}}] \quad (2)$$

where a shear strength, $\tau$, evolves towards a residual value over a time scale, $t^*$, and $f = f(\text{slip})$ linearly decreases from $f_s$ to $f_d$ as slip accumulates. This is a simplified form of that suggested by *Prakash and Clifton* [1993] and *Prakash* [1998], which was investigated for its stability properties in *Ranjith and Rice* [2001] and implemented in *Cochard and Rice* [2000]. Ideally $t^*$ should be much larger than the numerical time step, $\Delta t$, yet much smaller than the time, $T$, to undergo slip weakening. Here we use, $t^* = 2\Delta x/C_{s1}$ and $4\Delta x/C_{s1}$, for the elastic-plastic and elastic models, respectively, where $\Delta x$ is the element dimension in the direction of slip and $C_{s1}$ is the shear wave speed of material 1. We use a smaller $t^*$ for the elastic-plastic models because the inclusion of off-fault deformation helps impede the growth of perturbations within the model domain. The stable time step can be approximated by $\Delta t = \Delta x/\sqrt{2}C_{p2}$, where $C_{p2}$ is the dilatational wave speed of material 2. While the time to undergo slip weakening depends on the rupture velocity, it is of the order $T = R_0/V_r \approx 40\Delta x/C_{s1}$, where 40 is determined by the grid resolution. These parameter choices result in $t^* = 6\text{-}12\Delta t$ and $T = 20\text{-}10t^*$, so the constraints on $t^*$ are satisfied.

Rupture is nucleated by the forced expansion of a crack [*Andrews*, 1985; *Dunham and Rice*, 2008]. Nucleation starts with weakening at a point and then forcing the growth of the weakened region by prescribing a lower frictional strength over a growing patch, expanding at some constant low speed. This expansion occurs until the weakened region attains an unstable size, and spontaneous rupture ensues at much higher speed.

### 2.2. Off-Fault Elastic-Plastic Material

We use the pressure dependent Drucker-Prager yield criterion, which is given by

$$\overline{\tau} + \mu(\sigma_{kk}/3) = b \quad (3)$$

where $b$ is the cohesion, $\mu$ is the slope of the yield surface, and $\overline{\tau} = \sqrt{(1/2)s_{ij}s_{ij}}$ is the square root of the second invariant of the deviatoric stress $s_{ij} = \sigma_{ij} - \delta_{ij}\sigma_{kk}/3$. For the initial stress states used here, with $\sigma_{33}^0 = (\sigma_{11}^0 + \sigma_{22}^0)/2$, the Drucker-Prager yield criterion coincides exactly with the Mohr-Coulomb criterion as discussed by *Templeton and Rice* [2008].

We use a yield surface slope $\mu = 0.51$, which is analogous to a material with a Mohr-Coulomb coefficient of friction of $\tan\phi = 0.6$ (using the relation $\mu = \sin\phi$). This value for $\mu$ corresponds to the static coefficient of friction, $f_s = 0.6$, on the fault. As in *Templeton and Rice* [2008], we assume that this is a mature fault that has experienced multiple ruptures. This has resulted in the fault being surrounded by a zone of highly damaged rock, which we idealize as cohesionless, and thus we prescribe a negligible level of cohesion, $b = 10^{-6}\sigma_n$ ($b = 0$ is not an admissible parameter in the program).

We also allow dilatancy to occur during the plastic deformation. We define the dilatancy factor, $\beta$, as the ratio of an increment of volumetric plastic strain, $d\epsilon_{kk}^{pl}$, to an increment of shear plastic strain, $d\gamma^{pl}$

$$\beta = \frac{d\epsilon_{kk}^{pl}}{d\gamma^{pl}} \quad (4)$$

where $d\gamma^{pl} = \sqrt{2\,de_{ij}^{pl}\,de_{ij}^{pl}}$, and $de_{ij}^{pl} = \epsilon_{ij}^{pl} - \delta_{ij}\epsilon_{kk}/3$. We investigate a range of dilatancy values, ranging from non-dilative ($\beta = 0$) to associated flow ($\beta = \mu$), to asses the role of this parameter (see table 1 for a complete list of parameters). *Rudnicki and Rice* [1975] inferred from the data of

*Brace et al.* [1966] on cracked crystalline rocks, that $\beta$ was in the range of 0.2-0.4, which is roughly half of the value inferred for $\mu$.

## 3. Results

The results of the parameter study are summarized in table 2, where we see the important role that $\Psi$ plays in determining the preferential rupture direction. The preference for one direction over another is determined by a comparison of the rupture propagation velocity and slip velocity in each direction. The slip velocity varies with distance from the rupture tip, and it is highest just behind the rupture tip; it is this maximum value that we compare between the two directions of propagation. Frequently, both the rupture propagation velocity and slip velocity are higher in the same propagation direction, and in this situation the preferred rupture propagation direction is clear. In these cases, the result is denoted by an "R" or "L" for preferential propagation to the right or left, respectively, for the right-lateral rupture examined (note that a mark of "R" or "L" does not necessarily indicate unilateral rupture propagation). Additionally, the difference between the rupture velocities in the two directions is quantified by the quantity

$$\overline{V} \equiv \frac{V_+ - V_-}{V_+ + V_-} \quad (5)$$

where $V_+$ is the rupture velocity towards the right, and $V_-$ is the velocity towards the left, both of which are non-negative quantities. $\overline{V}$ ranges from $-1 \leq \overline{V} \leq 1$, where $\overline{V} = 1$ indicates unilateral rupture to the right, $\overline{V} = -1$ indicates unilateral rupture to the left, $\overline{V} = 0$ indicates a symmetric rupture, and $0 < |\overline{V}| < 1$ indicates a bilateral rupture with a faster rupture velocity in one direction over another.

Often the preferred direction indicated by the slip and rupture velocities will not agree, and the result is denoted by "r/l", where the first letter denotes the preferred direction based on the slip velocity, and the second letter indicates the preferred direction based on the rupture velocity. The value for $\overline{V}$ is also included in these cases to show the magnitude of the rupture velocity contrast.

Sometimes the rupture fails to propagate in one or both of the directions, or it can be highly delayed in one direction. If the rupture only grows through the forced expansion of the nucleation crack during the model time, and reaches a crack length greater than $30R_0$ without spontaneous propagation, the result is denoted with a "(—)". Generally, as the nucleation crack expands, rupture begins to dynamically propagate to the right slightly before it propagates to the left, but in some cases, the leftward rupture is highly delayed. If the rightward rupture reaches a rupture velocity of $V_r \geq 0.80C_{s1}$ before the leftward rupture starts to dynamically propagate, the result is denoted with a superscript "2" in table 2.

When off-fault plastic deformation is included, we report contours of accumulated plastic strain, $\gamma_{eq}^{pl}$, where

$$\gamma_{eq}^{pl} = \int_0^t \frac{d\gamma^{pl}}{dt'} dt' \quad (6)$$

and $d\gamma^{pl}$ is defined as above.

The following sections describe the role that the stiffness contrast, $S$ ratio, principal stress orientation, $\Psi$, and dilatancy, $\beta$, play in controlling the preferred rupture direction and location of off-fault deformation.

## 3.1. Rupture with Elastic Off-Fault Response

In the case of rupture on a bimaterial interface between elastic media, there is preference for rupture to propagate in one direction or another dependent on the $S$ ratio, but there is no dependence on $\Psi$. Figure 2a-c shows the rupture propagation for an $S$ ratio of 2.0. The slip distribution (figure 2a) is asymmetric, reflecting a faster propagation towards the right. The preferential propagation to the right can be seen by looking at both the rupture velocity and the slip velocity (figure 2b and c), which are both higher for propagation towards the right. This is the direction predicted by *Ben-Zion* [2001], with slip in the more compliant side of the fault, also called the positive direction. For $S = 2.0$, the value for $\overline{V}$ is positive, indicating faster rupture propagation to the right, but $\overline{V} < 1$, because the rupture is bilateral.

Figure 3a shows the change in normal stress on the fault as the rupture propagates. For propagation to the right, the preferred direction, the normal stress decreases (becomes less compressive) as the fault begins to slip, but increases ahead of the rupture tip, in agreement with previous work [e.g., *Andrews and Ben-Zion*, 1997; *Rubin and Ampuero*, 2007]. For these crack-like ruptures, the normal stress decrease can continue to grow and fault opening can occur. For propagation to the left, the normal stress changes are reversed; the normal stress decreases ahead of the rupture tip and increases as slip begins to accumulate. We note that the results presented here do not depend on the choice of regularization time scale, $t^*$, but larger values for $t^*$ will damp the oscillations seen in the normal stress. We have examined the rupture behavior for $t^* = 2$, 4, and $6\Delta x/C_{s1}$ and found no change in the direction of preferential propagation, although the fault does open for smaller crack lengths with a smaller value for $t^*$.

If the $S$ ratio is lowered to 1.4, which brings the fault closer to failure, the behavior is largely the same as for the aforementioned case of $S = 2.0$. The slip velocity is higher for propagation towards the right, but the difference in rupture velocities is very small (with $\overline{V} \sim 0$) and more pronounced when the $S$ ratio is higher. If the $S$ ratio is further reduced to 0.8, the fault is brought closer to failure, and rupture propagates at a supershear velocity towards the left and at a subshear velocity to the right (figure 2d-f). Figure 2 shows some of the complexities involved with bimaterial ruptures; as the normal stress changes behind the rupture tip, the fault is able to open. The rupture towards the left is like a phase identified by *Ranjith and Rice* [2001] and simulated by *Cochard and Rice* [2000]. Towards the left, the normal stress is decreased ahead of the crack tip, and increased in the slip-weakening zone close-up, due to the bimaterial effect. This decrease ahead of the tip contributes to an easy transition to a supershear velocity. While the rupture velocity is greater towards the left, the slip velocity is still higher for the rupture tip that is propagating towards the right, prior to the fault opening.

These observations of bilateral rupture and changes in rupture propagation as the $S$ ratio is varied are consistent with the experiments of *Xia et al.* [2005], who always observed bilateral rupture and found that the direction of preferential rupture propagation was dependent on the level of shear prestress. This is also consistent with *Harris and Day* [1997], who observed bilateral rupture propagation in numerical simulations for a range of material contrasts.

## 3.2. Elastic-Plastic Influence of $S$ Ratio

The $S$ ratio significantly affects the rupture propagation with a purely elastic off-fault response and it can also alter the rupture behavior with an elastic-plastic off-fault material. The most apparent effect of changing the $S$ ratio is a change in the extent of plastic deformation, as seen in figure 4a-c. A larger zone of plastic deformation exists for lower $S$ ratios, but the side of the fault on which most of the plastic deformation accumulates is not influenced by the $S$ ratio. As discussed by *Templeton and Rice* [2008], as the $S$ ratio is lowered, the fault is loaded closer to failure and the stress state of the material off the fault is also moved closer to the yield surface. Therefore, lower $S$ ratios lead to more extensive deformation off the fault. This is true for all values of dilatancy investigated and all $\Psi$ values considered.

Changing the $S$ ratio also elucidates the cause of a temporal change in the rupture propagation, which is shown in the rupture velocity (figure 4d-f). When rupture first starts to accelerate ahead of the forcibly expanding crack, the rupture velocity is faster towards the right, but after some distance of propagation (shown by the vertical gray line in figures 4e and f), the rupture propagates faster towards the left. This transition may also be seen in the slip velocity snapshots. For most models, the slip velocity is initially higher towards the right, but depending on the stress state, this can flip after some distance of propagation.

This temporal change is the result of a switch between predominately elastic to elastic-plastic deformation. Initially, as the crack begins to accelerate, there is a negligible amount of off-fault plastic deformation, and the rupture behaves as it would elastically with preferential propagation towards the right. This propagation distance is labeled in figure 4a-c as the crack length before significant plastic deformation occurs; lower $S$ ratios lead to a smaller crack length. When plastic deformation becomes substantial, this behavior may change and the rupture may begin to propagate faster towards the left. The point at which the faster rupture velocity flips is proportional to the crack length when plastic deformation becomes non-negligible. This flip is not seen for the low $S$ ratio case ($S = 0.8$, figure 4d) because when the crack becomes large enough to accelerate, there is already substantial off-fault plastic deformation. This initial phase is not included in the table of results (table 2).

From table 2 we see that for $\Psi = 15°$, there is relatively little change in the final behavior by altering the $S$ ratio. The difference in final rupture velocity between the two propagation directions is larger for lower $S$ ratios, but the qualitative behavior is the same. For $\Psi = 35°$, the $S$ ratio plays a more significant role. As the $S$ ratio is increased, it is more likely that rupture will only propagate unilaterally during the model run time. For much longer run times, it is possible that the rupture will propagate in both directions, but this is only due to the continued forced expansion of the crack used to nucleate.

Changes in the $S$ ratio can have a significant effect for the case of $\Psi = 25°$, when the extent of plastic deformation is nearly identical on the compressional and extensional sides of the fault. For low $S$ ratios, the transition to supershear rupture towards the left, as seen in the purely elastic analysis, is able to occur. For larger $S$ ratios, the direction of preferential rupture propagation is not clear, because the slip and rupture velocities indicate opposite directions.

## 3.3. Elastic-Plastic Influence of $\Psi$ and $\beta$

We find that the orientation of the maximum principal compressive stress, $\Psi$, principally controls the location of plastic deformation. As $\Psi$ is increased from $15°$ to $35°$, the location of plastic deformation transitions from the compressive side of the fault to the extensional side (figure 5a). The distribution of deformation is qualitatively similar to that observed by *Templeton and Rice* [2008] and *Viesca et al.* [2008] for a homogenous model, but here a larger magnitude of deformation occurs in the more compliant material. This differs from the results of *Duan* [2008] who found a larger magnitude of plastic strain in the stiffer material.

The direction of preferential rupture propagation is highly influenced by the value of $\Psi$ (see table 2). For $\Psi = 15°$, rupture propagates bilaterally with a preference towards the left, but for $\Psi = 35°$ and $45°$, the rupture frequently propagates unilaterally towards the right. This is in agreement with the result of *Ben-Zion and Shi* [2005], who investigated the case of $\Psi = 45°$ and is consistent with off-fault deformation preferentially occurring in the stiffer material.

The details of the distribution of plastic deformation around the propagating rupture tip can be seen in figure 6. When $\Psi = 35°$, localizations in the plastic strain can be seen. The localizations are weak for the rupture propagating to the right, but they are prominent for the deformation to the left. In this case, the leftward rupture is not propagating dynamically, but is rather being forced to expand by the nucleation procedure.

These localizations are in accord with the established theory of *Rudnicki and Rice* [1975], which notes that there is a nonzero critical hardening, $h_{cr}$, for the plane strain conditions modeled here, below which (i.e., when $h < h_{cr}$) localization can develop. These localization features are not fully resolved and are expected to have an essential, if artificial, dependence on grid size. *Templeton and Rice* [2008] examine the grid size dependence and find that the dynamics of rupture propagation are not dependent on the grid size. By introducing some amount of hardening ($h > 0$), which shifts the yield surface away form the hydrostatic axis as plastic deformation accrues (see *Templeton and Rice* [2008] for a complete discussion), the localizations can be inhibited with little effect on the overall extent of the plastically deformed regions.

If localization is inhibited by introducing sufficient hardening, the rupture propagation can be slightly modified. For $S = 1.4$, $\Psi = 35°$, and $\beta = 0.26$, localization can occur (figure 5 and 6c) because there is no hardening ($h = 0$), and $h < h_{cr}$, where $h_{cr}$ depends on $\mu$, $\beta$, and on the ratios of principal stresses. Localization, for a given stress state, can be inhibited by increasing $h$, or suitably changing $\beta$ or $\mu$. After introducing such hardening, there are no localizations and there is only a minor change to the rupture propagation. With hardening, rupture towards the right requires a smaller initial crack size for dynamic propagation. Towards the left, with sufficient hardening, the rupture is able to dynamically propagate and can transition to supershear, but this rupture is highly delayed and only occurs long after rupture to the right begins to dynamically propagate.

The change in normal stress on the fault has the same character for the elastic-plastic and the elastic models (figure 3); to the right there is an increase in normal stress ahead of the rupture, a decrease as slip begins, and vice versa for propagation to the left. For the same crack length, the changes in fault normal stress are smaller in amplitude for the elastic-plastic versus the elastic model (figure 3). However, the rupture velocity is much slower, for the same crack length, for the elastic-plastic models. When off-fault deformation occurs, the rupture velocity also depends on $\Psi$. For large $\Psi$, a broader region undergoes plastic deformation. This increases the crack length required to initiate rupture and results in a slower rupture velocity for larger $\Psi$. Therefore, although figure 3 shows different levels of normal stress change, we find that for the same rupture velocity, the elastic and the elastic-plastic models have approximately the same amplitude of normal stress alteration.

Figure 7 shows how the plastic deformation changes as the dilatancy of the material is altered. For a non-dilative material ($\beta$=0.0, figure 7a), there is significant strain localization. Since hardening is not included here, localization occurs, but can be inhibited by increasing the dilatancy, $\beta$, which reduces the level of critical hardening. As the dilatancy is increased up to $\beta = 0.51$ (associated flow), the details of the plastic deformation for the rightward rupture

change. However, the bulk distribution and magnitude is not significantly sensitive to the value of the dilatancy parameter. The distribution of plastic deformation changes for the leftward rupture because as $\beta$ increases, the rupture is able to transition to supershear, and the plastic deformation is showing this transition (figure 7d).

Table 2 illustrates the sensitivity of the results to changes in dilatancy. For $\Psi = 35°$ and $45°$ and a non-dilative material ($\beta = 0$), the rupture does not spontaneously propagate during the model run time and there are significant localizations of plastic deformation around the forcibly expanding crack. For the highly dilative case ($\beta = 0.51$), there are no strain localizations and the rupture propagates bilaterally.

For $\Psi = 15°$, the rupture propagates bilaterally for all dilatancy values investigated and the preferential direction is reversed with both higher slip and rupture velocities towards the left. With less dilation this effect is more pronounced and there are larger differences in rupture velocities.

The results for $\Psi = 25°$ are intermediate to the cases of $\Psi = 15°$ and $35°$. The rupture velocity is generally higher towards the left while the faster slip velocities are found towards the right.

With the inclusion of off-fault deformation, a dependence on $\Psi$ is introduced and rupture can preferentially travel in either direction depending on this parameter. For high angles of $\Psi$, rupture preferentially travels towards the right, i.e., in the direction of slip in the more compliant material, and can result in plastic deformation occurring only in the stiffer material. For low angles of $\Psi$, however, rupture propagates bilaterally, with a preference for propagation towards the left. Plastic deformation occurs in the compressional quadrant for low $\Psi$, which for propagation towards the left, also results in plastic deformation in the stiffer material.

## 4. Discussion and Conclusions

The purely elastic models show bilateral propagation and include a preferential rupture propagation towards the right for an $S$ ratio of 2.0 and a supershear rupture propagation towards the left for an $S$ ratio of 0.8. This reflects the range of behaviors that were observed by *Xia et al.* [2005], who found that rupture was always bilateral and that the direction of preferential propagation was dependent level of initial shear stress on the fault. They found that rupture can either propagate in both directions with a subshear rupture velocity, or, for cases which were loaded closer to incipient sliding (i.e. a lower $S$ ratio), they found that the rupture traveled faster than the shear wave speed of both materials in the direction of slip in the stiffer material (to the left in our model setup). This is consistent with the differences in behavior that we see for the elastic cases with $S$ ratios of 0.8 and 2.0.

When off-fault deformation is allowed to occur, a dependence on $\Psi$ is introduced. The range in $\Psi$ that we investigate here represents a range of tectonic environments. High values of $\Psi$ are found around the San Andreas fault [*Zoback et al.*, 1987; *Hardebeck and Hauksson*, 2001; *Townend and Zoback*, 2004]. While values of $\Psi \geq 45°$ are expected around the major, active strike-slip faults of California, a large range of values for $\Psi$ are relevant to strike-slip settings as faults rotate into and out of an optimal orientation for failure over geologic time [*Nur and Ron*, 2003].

For high angles of $\Psi$, relevant for the strike-slip settings examined by *Ben-Zion and Shi* [2005], rupture preferentially travels in the positive direction, towards the right, i.e., in the direction of slip in the more compliant material. The plastic behavior (the dilatancy value, $\beta$) does not change the preferred direction, but the preference for one direction over the other can be enhanced with less material dilation. For these stress states, most plastic deformation occurs in

the extensional quadrant. For the range in dilatancy values investigated, rupture will often propagate unilaterally towards the right, and in these scenarios, plastic deformation will only occur in the stiffer material. This is consistent with the analyses of *Ben-Zion and Shi* [2005] who used a value for $\Psi$ of $45°$.

For low angles of $\Psi$, however, rupture propagates bilaterally, with a preference for propagation in the negative direction, towards the left. Low values for $\Psi$ (such as $\Psi = 15°$) are expected in subduction zone settings, where the subduction interface dip is shallow, 1-15°, and the maximum compressive stress is approximately horizontal [e.g., *Clift and Vannuchi*, 2004]. Given the material contrast present in a subduction zone, a preference for the negative direction is preferential propagation downdip. The case of $\Psi = 15°$ is also relevant to the basal fault that may underlie thin skinned fold-and-thust belts, but larger values, such as $\Psi = 25°$ or $35°$, characteristic of traditional Andersonian faulting, are relevant for the faults that are interior to a fold-and-thrust belt [e.g., *Suppe*, 2007; *Hubbard et al.*, 2010]. For low $\Psi$, plastic deformation occurs in the compressional quadrant, which for propagation towards the left, also results in plastic deformation in the stiffer material.

The dependence of the preferred propagation direction on $\Psi$ is a result of the fact that $\Psi$ controls whether plastic deformation occurs on the compressive or extensional side of the fault [*Templeton and Rice*, 2008]. When rupture propagates bilaterally, a larger magnitude of plastic deformation occurs in the more compliant material, regardless of the value of $\Psi$. A larger magnitude of plastic deformation means that more energy is being used to plastically deform the material, and this results in a lower rupture velocity. Therefore, since $\Psi$ determines if propagation in a given direction will plastically deform the stiffer or the more compliant material, $\Psi$ influences the direction in which the rupture will preferentially propagate.

We find that only for the higher angles of $\Psi$ investigated, $\Psi \geq 35°$, can the observations of *Dor et al.* [2006] hold that more deformation will occur in the material with the faster seismic velocity. Then the rupture propagation is typically unilateral, in the direction of slip in the more compliant material, as found by *Ben-Zion and Shi* [2005]. However, we see that ruptures are often not unilateral for low $\Psi$ and the magnitude of plastic deformation is greater in the more compliant material, so that the aforementioned observations would not be expected to be made in such cases.

Given the scenarios investigated here, we find that an observation of asymmetry of damage cannot, by itself, be evidence of a rupture propagation direction with slip in the more compliant material. The location of deformation depends not only on the material contrast, but also on the orientation of the principal stresses as well as their relative magnitude and how close the fault and surrounding material are to failure. Knowledge of the stress state, as provided in the studies of *Zoback et al.* [1987], *Hardebeck and Hauksson* [2001] and *Townend and Zoback* [2004], must be used in conjunction with the observed plastic deformation to assess the likelihood of unilateral rupture in a specified direction.

Other sources of asymmetry across the fault, such as the effect of a dipping fault in the presence of a free surface [e.g., *Oglesby et al.*, 1998], can further alter the stress state around the propagating rupture tip and can either reinforce or dampen the asymmetry of the bimaterial propagation, depending on the model setup [*Ma and Beroza*, 2008]. *Ma* [2009] show that the characteristics of plastic deformation around a dipping fault can be significantly different from the model here, with no free surface. Incorporating these effects into the framework will provide further insight into the accumulation of plastic deformation in thrust or normal faulting regimes, but may not be helpful for understanding the strike-slip setting as *Ma and Andrews* [2010] show that the characteristics of the plastic deformation are qualitatively similar with depth, except very near the surface.

Our work indicates that it is not always straightforward to associate rupture directivity only with bimaterial contrast. This is unfortunate given that mechanically correct predictions of directivity, under particular tectonic conditions, would be extremely valuable in light of the dependence of ground shaking on rupture directivity. For example, depending on the directivity of rupture on the southern San Andreas fault, either the Los Angeles basin or Mexicali will be strongly affected [*Olsen et al.*, 2006], but material contrast alone, independent of constraints on prestress, cannot predict this.

# References

Adams, G. G. (1995), Self-excited oscillations of two elastic half-spaces sliding with a constant coefficient of friction, *J. Appl. Mech.*, *62*, 867–872.

Adams, G. G. (2001), An intersonic slip pulse at a frictional interface between dissimilar materials, *J. Appl. Mech.*, *68*, 81–86, doi:10.1115/1.1349119.

Andrews, D. J. (1976), Rupture velocity of plane strain shear cracks, *J. Geophys. Res.*, *81*(32), 5679–5687.

Andrews, D. J. (1985), Dynamic plane-strain shear rupture with a slip-weakening friction law calculated by a boundary integral method, *Bull. Seis. Soc. Am.*, *75*(1), 1–21.

Andrews, D. J., and Y. Ben-Zion (1997), Wrinkle-like slip pulse on a fault between different materials, *J. Geophys. Res.*, *102*(B1), 553–571.

Andrews, D. J., and R. A. Harris (2005), The wrinkle-like slip pulse is not important in earthquake dynamics, *Geophys. Res. Lett.*, *32*, L23,303, doi:10.1029/2005GL023996.

Ben-Zion, Y. (2001), Dynamic ruptures in recent models of earthquake faults, *J. Mech. Phys. Solids*, *49*, 2209–2244.

Ben-Zion, Y. (2006a), Comment on "Material contrast does not predict earthquake rupture propagation direction" by R. A. Harris and S. M. Day, *Geophys. Res. Lett.*, *33*, L13,310, doi:10.1029/2005GL025652.

Ben-Zion, Y. (2006b), Comment on "The wrinkle-like slip pulse is not important in earthquake dynamics" by D. J. Andrews R. A. Harris, *Geophys. Res. Lett.*, *33*, L06,310, doi:10.1029/2005GL025372.

Ben-Zion, Y., and D. J. Andrews (1998), Properties and implications of dynamic rupture along a material interface, *Bull. Seis. Soc. Am.*, *88*(4), 1085–1094.

Ben-Zion, Y., and Z. Shi (2005), Dynamic rupture of a material interface with spontaneous generation of plastic strain in the bulk, *Earth Planet. Sci. Lett.*, *236*, 486–496.

Brace, W. F., B. W. Paulding, and C. Scholz (1966), Dilatancy in fracture of crystalline rocks, *J. Geophys. Res.*, *71*, 3939–3953.

Clift, P., and P. Vannuchi (2004), Controls on tectonic accretion versus erosion in subduction zones: Implications for the origin and recycling of the continental crust, *Rev. of Geophys.*, *42*, RG2001, doi:10.1029/2003RG000127.

Cochard, A., and J. R. Rice (2000), Fault rupture between dissimilar materials: Ill-posedness, regularization and slip-pulse response, *J. Geophys. Res.*, *105*(B11), 25,891–907.

Dalguer, L. A., and S. M. Day (2009), Asymmetric rupture of large aspect-ratio faults at bimaterial interface in 3D, *Geophys. Res. Lett.*, *36*, L23,307, doi:10.1029/2009GL040303.

Das, S., and K. Aki (1977), A numerical study of two-dimensional spontaneous rupture propagation, *Geophys. J. R. astr. Soc.*, *50*, 643–668.

Dor, O., T. K. Rockwell, and Y. Ben-Zion (2006), Geological observations of dsamage asymmetry in the structure of the San Jacinto, San Andreas and Punchbowl faults in southern Calicornia: A possible indicator for preferred rupture propagationdirection, *Pure. Appl. Geophys.*, *163*, 301–349, doi:10.1007/s00024-005-0023-9.

Duan, B. (2008), Asymmetric off-fault damage generated by bilateral ruptures along a bimaterial interface, *Geophys. Res. Lett.*, *35*, L14,306, doi:10.1029/2008GL034797.

Dunham, E. M., and J. R. Rice (2008), Earthquake slip between dissimilar poroelastic materials, *J. Geophys. Res.*, *113*, B09,304, doi:10.1029/2007JB005405.

Fuis, G. S., et al. (2003), Fault systems of the 1971 San Fernando and 1994 Northridge earthquakes, southern California: Relocated aftershocks and seismic images from LARSE II, *Geology*, *31*(2), 171–174.

Hardebeck, J. L., and E. Hauksson (2001), Crustal stress field in southern California and its implications for fault mechanics, *J. Geophys. Res.*, *106*(B10), 21,859–21,882.

Harris, R. A., and S. M. Day (1997), Effects of a low-velocity zone on a dynamic rupture, *Bull. Seis. Soc. Am.*, *87*(5), 1267–1280.

Harris, R. A., and S. M. Day (2005), Material contrast does not predict earthquake rupture propagation direction, *Geophys. Res. Lett.*, *32*, L23,301, doi:10.1029/2005GL023941.

Hubbard, J., J. H. Shaw, and Y. Klinger (2010), Structural setting of the 2008 $m_w$ 7.9 Wenchuan, China, earthquake, *Bull. Seis. Soc. Am.*, *100*(5B), 2713–2735, doi:10.1785/0120090341.

Ida, Y. (1972), Cohesive force across the tip of a Longitudinal-Shear crack and Griffith's specific surface energy, *J. Geophys. Res.*, *77*(20), 3796–3805.

Ma, S. (2009), Distinct asymmetry in rupture-induced inelastic strain across dipping faults: An off-fault yielding model, *Geophys. Res. Lett.*, *36*, L20,317, doi:10.1029/2009GL040666.

Ma, S., and D. J. Andrews (2010), Inelastic off-fault response and three-dimensional dynamics of earthquake rupture on a strike-slip fault, *J. Geophys.Res.*, *115*, B04,304, doi: 10.1029/2009JB006382.

Ma, S., and G. C. Beroza (2008), Rupture dynamics on a bimaterial interface for dipping faults, *Bull. Seis. Soc. Am.*, *98*(4), 1642–1658, doi:10.1785/0120070201.

Nur, A., and H. Ron (2003), Material and stress rotations: The key to reconciling crustal faulting complexity with rock mechanics, *Inter. Geol. Rev.*, *45*(8), 671–690.

Oglesby, D. D., R. J. Archuleta, and S. B. Nielsen (1998), Earthquakes on dipping faults: The effects of broken symmetry, *Science*, *280*, 1055–1059.

Olsen, K. B., S. M. Day, J. B. Minster, Y. Cui, A. Chourasia, M. Faerman, R. Moore, P. Maechling, and T. Jordan (2006), Strong shaking in Los Angeles expected from southern San Andreas earthquake, *Geophys. Res. Lett.*, *33*, L07,305.

Palmer, A. C., and J. R. Rice (1973), Growth of slip surfaces in progressive failure of over-consolidated clay, *Proceedings of the Royal Society of London Series A-Mathematical Physical and Engineering Sciences*, *332*(1591), 527–548.

Poliakov, A. N. B., R. Dmowska, and J. R. Rice (2002), Dynamic shear rupture interactions with fault bends and off-axis secondary faulting, *J. Geophys. Res.*, *107*(B11), 2295, doi: 10.1029/2001JB000572.

Prakash, V. (1998), Frictional response of sliding interfaces subjected to time varying normal pressures, *J. of Tribol.*, *120*, 97–102, doi:10.1115/1/2834197.

Prakash, V., and R. J. Clifton (1993), Time resolved dynamic friction measurements in pressure-shear, in *Experimental Techniques in the Dynamics of Deformable Solids*, edited by A. K. T. Ramesh, pp. 33–48, Appl. Mech. Div., Am. Soc. of Mechanical Eng., Ney York.

Ranjith, K., and J. R. Rice (2001), Slip dynamics at an interface between dissimilar materials, *J. Mech. Phys. Solids*, *49*, 341–361.

Renardy, M. (1992), Ill-posedness at the boundary for elastic solids sliding under coulomb friction, *J. of Elasticity*, *27*, 281–287.

Rice, J. R., C. G. Sammis, and R. Parsons (2005), Off-fault secondary failure induced by a dynamic slip pulse, *Bull. Seis. Soc. Am.*, *95*(1), 109–134, doi:10.1785/0120030166.

Rubin, A. M., and J.-P. Ampuero (2007), Aftershock asymmetry on a bimaterial interface, *J. Geophys. Res.*, *112*, B05,307, doi:10.1029/2006JB004337.

Rudnicki, J. W., and J. R. Rice (1975), Conditions for localization of deformation in pressure-sensitive dilatant materials, *Journal of the Mechanics and Physics of Solids*, *23*, 371–394.

Simones, F. M. F., and J. A. C. Martins (1998), Instability and ill-posedness in some friction problems, *Int. J. Eng. Sci.*, *36*, 1265–1293.

Suppe, J. (2007), Absolute fault and crustal strength from wedge tapers, *Geology*, *35*(12), 1127–1130, doi:10.1130/G24053A.1.

Takahashi, N., et al. (2002), Seismic structure of western end of the Nankai trough seismogenic zone, *Journal Geophys. Res.*, *107*, B102,212, doi:10.1029/2000JB000121.

Templeton, E. L., and J. R. Rice (2006), Extent and distribution of off-fault plasticity during seismic rupture including bimaterial effects, *EOS Trans. Amer. Geophys. Union*, *87*(52), fall Meet. Suppl., Abstract S34A-01.

Templeton, E. L., and J. R. Rice (2008), Off-fault plasticity and earthquake rupture dynamics: 1. Dry materials or neglect of fluid pressure changes, *J. Geophys. Res.*, *113*, B09,306, doi: 10.1029/2007JB005529.

Townend, J., and M. D. Zoback (2004), Regional tectonic stress near the San Andreas fault in central and southern California, *Geophys. Res. Lett.*, *31*(L15S11), doi:10.1029/2003GL018918.

Viesca, R. C., E. L. Templeton, and J. R. Rice (2008), Off-fault plasticity and earthquake rupture dynamics: 2. Effects of fluid saturation, *J. Geophys. Res.*, *113*, B09,307, doi: 10.1029/2007JB005530.

Weertman, J. (1980), Unstable slippage across a fault that separates elastic media of different elastic constants, *J. Geophys. Res.*, *85*, 1455–1461.

Xia, K., A. J. Rosakis, H. Kanamori, and J. R. Rice (2005), Laboratory earthquakes along inhomogeneous faults: Directionality and supershear, *Science*, *308*, 681–684.

Zoback, M. D., et al. (1987), New evidence on the state of stress of the San Andreas fault system, *Science*, *238*(4830), 1105–1111.

Nora DeDontney, Dept. of Earth and Planetary Sciences, Harvard Univ., 20 Oxford St., Cambridge MA 02138, USA. (ndedontn@fas.harvard.edu)

Elizabeth Templeton-Barrett, School of Engineering and Applied Sciences, Harvard University, now at ExxonMobil Upstream Research Company, Houston TX 77098, USA.

James R. Rice, Dept. of Earth and Planetary Sciences and School of Engineering and Applied Sciences, Harvard Univ., Cambridge MA 02138, USA.

Renata Dmowska, School of Engineering and Applied Sciences, Harvard Univ., Cambridge MA 02138, USA.
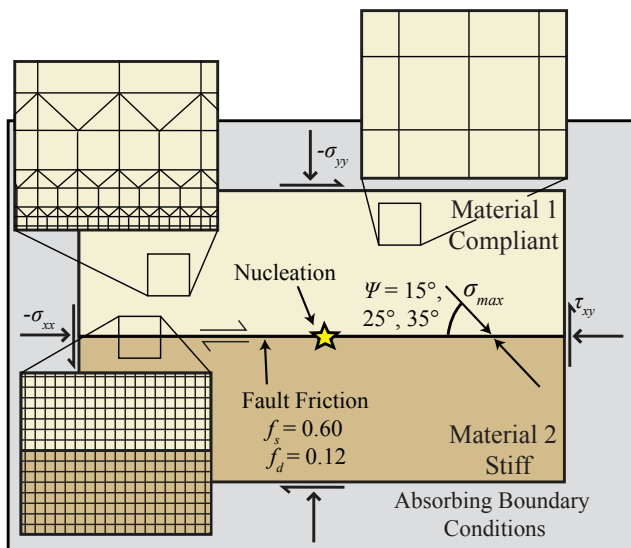
**Figure 1.** Model setup showing mesh geometry (with element size increasing with distance from the fault), material contrast, and definition of $\Psi$, which characterizes the orientation of the stress loading.

## Elastic, $S = 2.0$

a)

Slip, $s/D_c$

Slip in stiffer material ← → Slip in more compliant material

$x/R_0$

b)

Slip Velocity, $v/C_{pl} * 10^3$

$x/R_0$

c)

Rupture Velocity, $V_r/C_{sl}$

— Rupture to the right
- - Rupture to the left

$x/R_0$

## Elastic, $S = 0.8$

d)

Slip, $s/D_c$

$x/R_0$

e)

Slip Velocity, $v/C_{pl} * 10^3$

Supershear Transition

Fault Opens

$x/R_0$

f)

Rupture Velocity, $V_r/C_{sl}$

— Rupture to the right
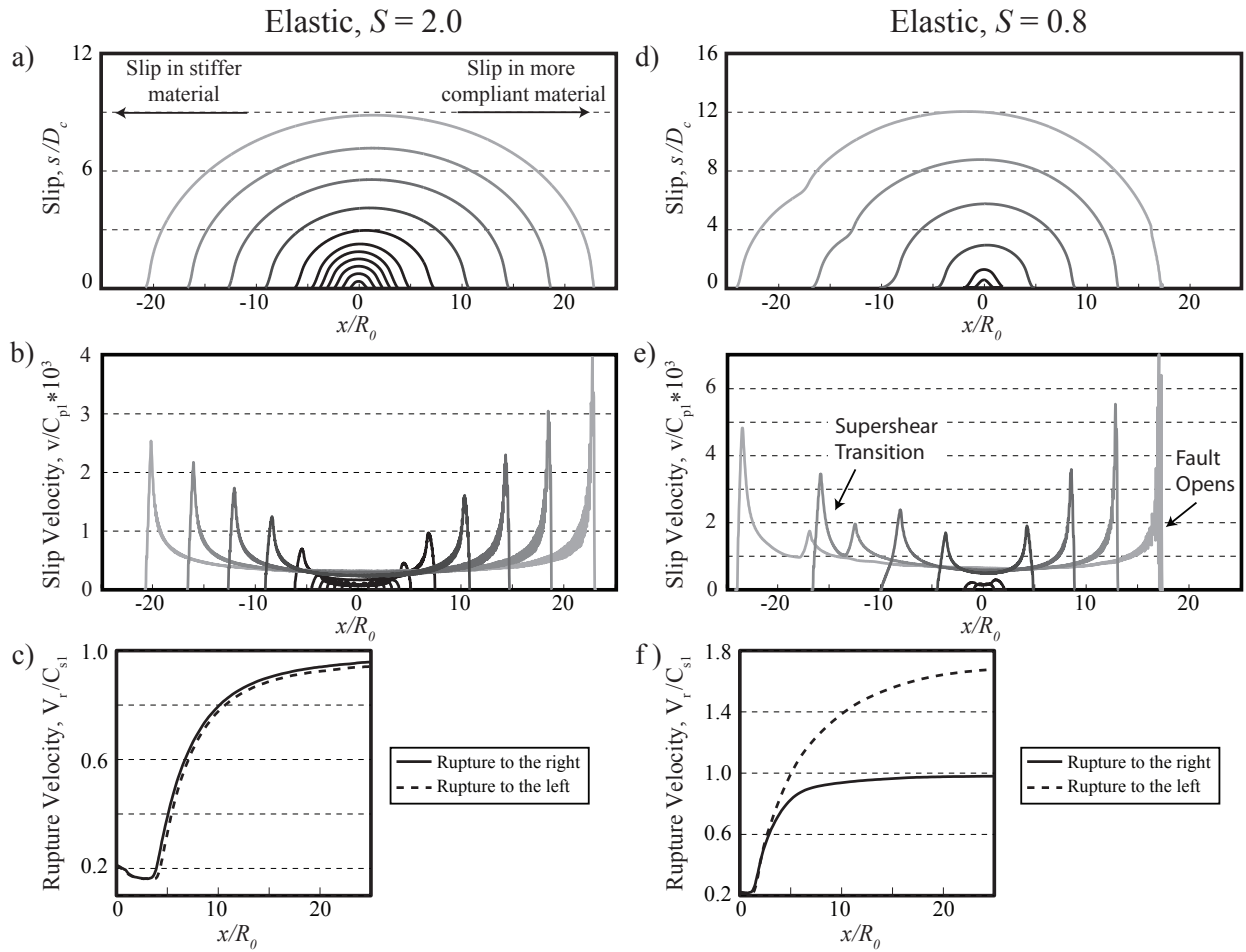- - Rupture to the left

$x/R_0$

**Figure 2.** For an elastic off-fault material, the $S$ ratio affects the rupture propagation. (a) and (d) Slip distribution. Lines are plotted for equal time steps. (b) and (e) Slip velocity. For both $S$ ratios, there is a higher peak slip velocity for rupture traveling towards the right. (c) and (f) Rupture velocity in both directions. For an $S$ ratio of 2.0, (a) - (c), rupture preferentially travels towards the right, with slip in the more compliant material, while for an $S$ ratio of 0.8, the propagation is more complex, and the leftward rupture transitions to supershear.
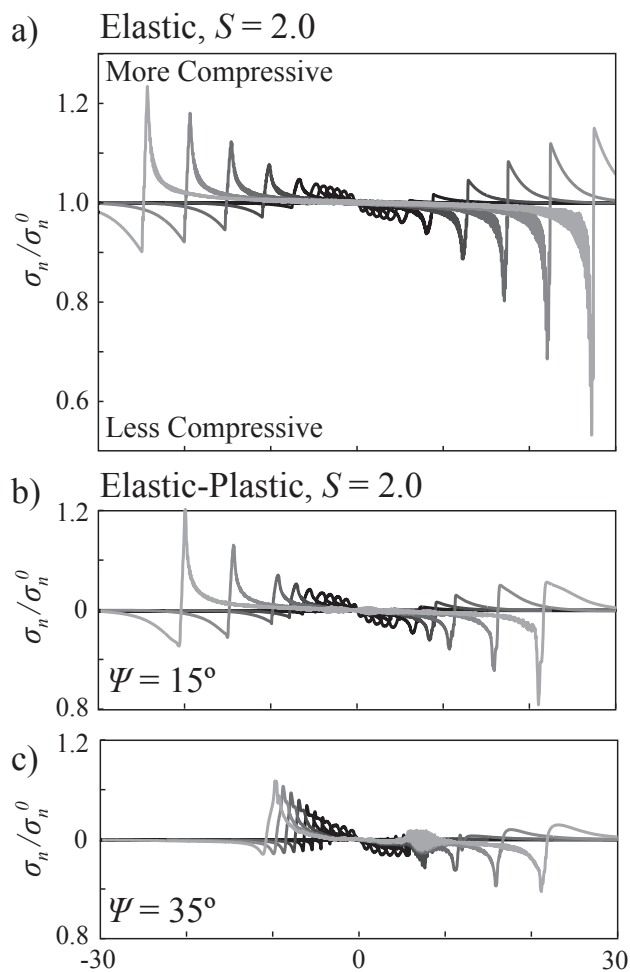
**Figure 3.** The contrast in elastic material properties across the fault results in a change in normal stress as the rupture propagates for both (a) elastic and (b)-(c) elastic-plastic models. Fault normal stress, $\sigma_n$, is normalized by the initial fault normal stress, $\sigma_n^0$.
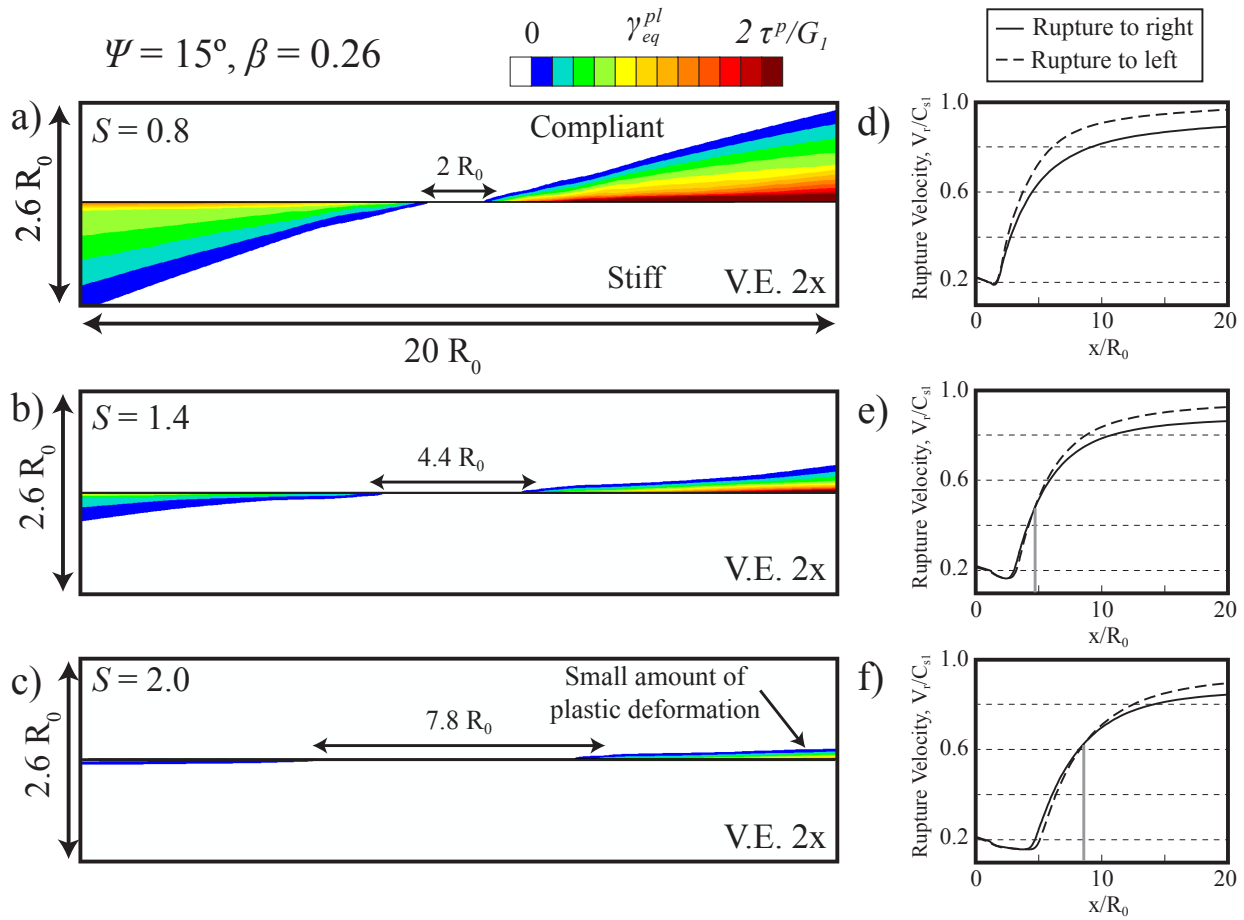
**Figure 4.** (a) - (c) Contours of plastic deformation show how the distribution of of off-fault plastic deformation changes with variations in the $S$ ratio. (Note: there is a 2x vertical exaggeration for easier viewing of the plastic zone.) Dimension labeled is the approximate crack length before significant plastic deformation occurs. (d) - (f) Rupture velocity in both directions for the different $S$ ratios examined. Vertical gray line denotes a transition from faster rupture velocity towards the right to towards the left.
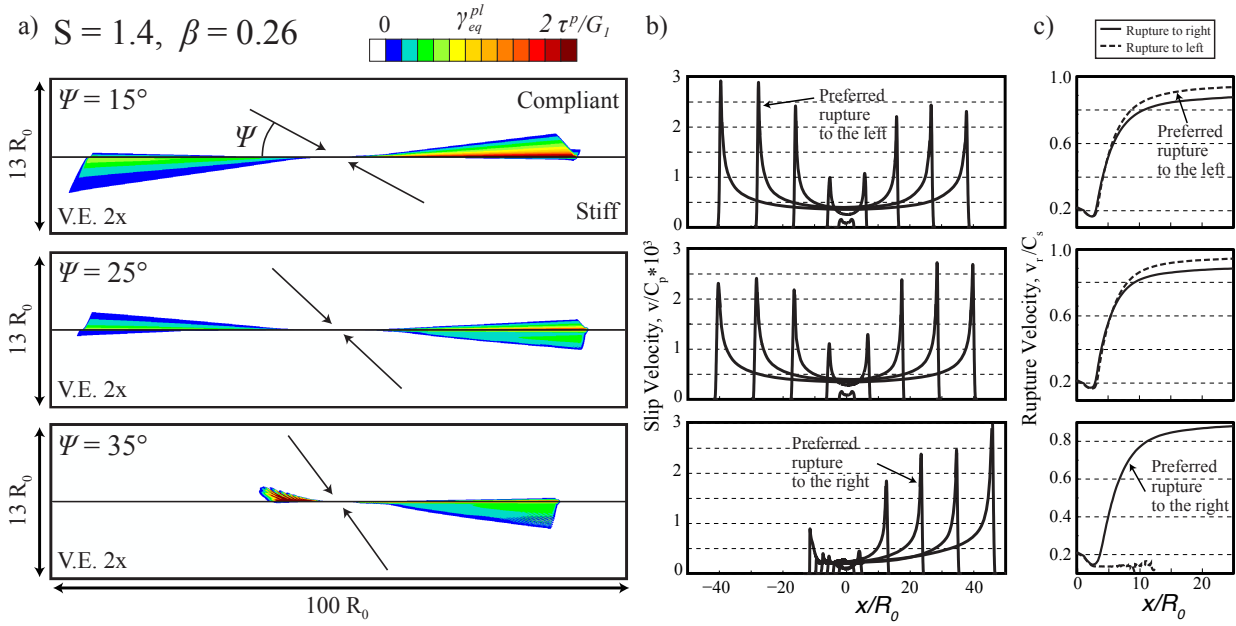
**Figure 5.** Changes in rupture propagation and plastic deformation result from changing $\Psi$. (a) Contours of plastic deformation. (Note: there is a 2x vertical exaggeration for easier viewing of the plastic zone, but which makes the $\Psi$ angle appear larger than actual.) (b) Slip velocity at different times during rupture (c) Rupture velocity to the right and left of the nucleation
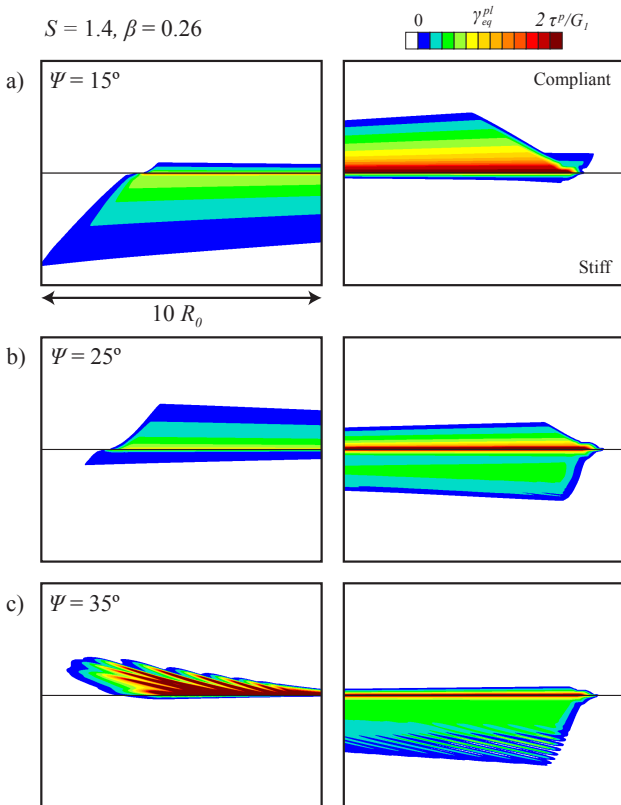


**Figure 6.** Close up of the plastic deformation around the rupture tip for the cases shown in figure 5.
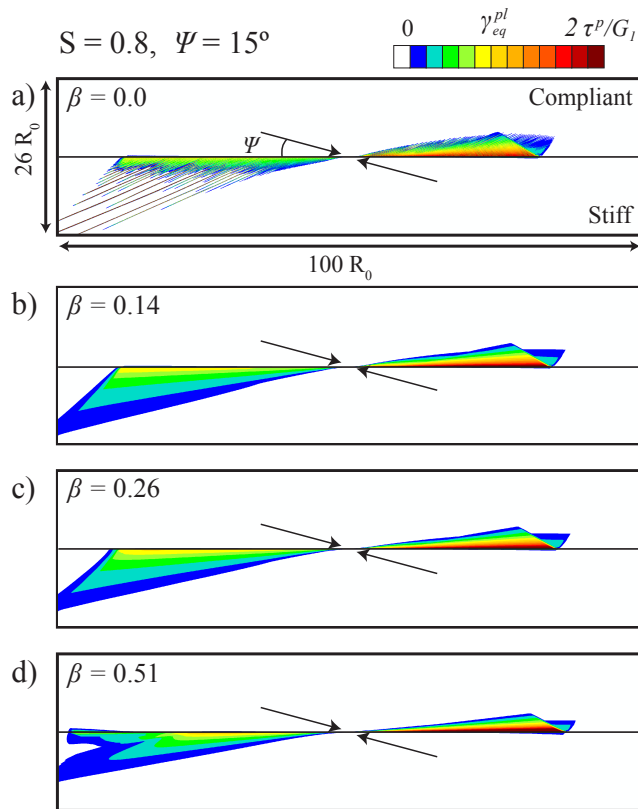
**Figure 7.** As the plastic dilation of the material is varied, the characteristics of the off-fault plastic deformation can change. (a) Non-dilative. (d) Associated flow. Rupture to right is subshear in all cases, rupture to the left subshear for (a) and (b) and transitions to supershear in (c) and (d).

**Table 1.** Material Parameters

| | | |
|---|---|---:|
| $\rho_1, \rho_2$ | Density | 2700, 3000 kg/m$^3$ |
| $E_1, E_2$ | Young's modulus | 60.8, 105.6 GPa |
| $G_1, G_2$ | Shear modulus | 24.3, 42.2 GPa |
| $\nu_1, \nu_2$ | Poisson's ratio | 0.25, 0.25 |
| $C_{p1}, C_{p2}$ | P wave speed | 5200, 6500 m/s |
| $C_{s1}, C_{s2}$ | S wave speed | 3002, 3753 m/s |
| $R_0$ | Slip-weakening zone size | 40 m |
| $f_s$ | Static friction | 0.6 |
| $f_d$ | Dynamic friction | 0.12 |
| $D_c$ | Slip-weakening length | 67 mm |
| $t^*$ | Regularized time scale | 6.66e-4 s |
| $\mu$ | Drucker-Prager internal friction | 0.51 |
| $\beta$ | Dilatancy parameter | 0, 0.14, 0.26, 0.51 |
| $b$ | Cohesion | $10^{-6}$ |

**Table 2.** Summary of results for the preferred rupture direction. The letter refers to the direction of preferred propagation (not the direction of unilateral propagation) and the number, $\overline{V}$, is a measure of the relative asymmetry in the velocity of rupture propagation (see equation (5)).

| $\Psi$ | $S$ Ratio | Elastic | | Elastic-Plastic | | | | | | |
|---|---|---|---|---|---|---|---|---|---|---|
| | | | | $\beta = 0.0$ | | $\beta = 0.14$ | | $\beta = 0.26$ | | $\beta = 0.51$ |
| | 0.8 | r/l | -0.27 | L | -0.04 | L | -0.05 | L | -0.04[1] | L | -0.04[1] |
| 15° | 1.4 | R | 0.0 | L | -0.04 | L | -0.04 | L | -0.04 | L | -0.03 |
| | 2.0 | R | 0.01 | L | -0.05 | L | -0.04 | L | -0.03 | L | -0.03 |
| | 0.8 | r/l | -0.27 | L | -0.29 | L | -0.29 | L | -0.28 | L | -0.27 |
| 25° | 1.4 | R | 0.0 | L | -0.19 | r/l | -0.04 | r/l | -0.03 | r/l | -0.03 |
| | 2.0 | R | 0.01 | (—) | | r/l | -0.03[2] | r/l | -0.06 | r/l | -0.02 |
| | 0.8 | r/l | -0.27 | R | 1.0 | R | 1.0 | r/l | -0.14[2] | r/l | -0.13 |
| 35° | 1.4 | R | 0.0 | (—) | | R | 1.0 | R | 1.0 | r/l | -0.12 |
| | 2.0 | R | 0.01 | (—) | | R | 1.0 | R | 1.0 | r/l | -0.12 |
| | 0.8 | r/l | -0.27 | (—) | | R | 1.0 | R | 1.0 | r/l[2] | -0.14 |
| 45° | 1.4 | R | 0.0 | (—) | | R | 1.0 | R | 1.0 | r/l[2] | -0.13 |
| | 2.0 | R | 0.01 | (—) | | (—) | | R | 1.0 | R[2] | 0.24 |

R : Rupture prefers to propagate to the right
L : Rupture prefers to propagate to the left
r/l : Slip velocity indicates preferred rupture towards the right while rupture velocity indicates preferred rupture to the left
(—) : Does not propagate in either direction
[1] Rupture to the left begins to transition to supershear
[2] Rupture to the left is highly delayed